EURASIAN PHYSICAL TECHNICAL JOURNAL

2026, Volume 23, No. 1 (55)

https://doi.org/10.31489/2026N1/145-153

Received: 21/11/2025 Revised: 18/02/2026 Accepted: 19/03/2026 Published online: 30/03/2026

Original Research Article

UDC 53.01:524.3-52

KINEMATIC ANALYSIS OF THE MASSIVE STAR-FORMING REGION G328.2551-0.5321 VIA ALMA MOLECULAR LINE OBSERVATIONS

Islyam Zh.B.[1], Nodyarov A.S.[1], Demessinova A.M.[1,*], Manapbayeva A.B.[1,2], Kyzgarina M.T.[1], Zhumabay N.[3]

[1] Al-Farabi Kazakh National University, Almaty, Kazakhstan
[2] Kazakh National Women's Teacher Training University, Almaty, Kazakhstan
[3] Abai Kazakh National Pedagogical University, Almaty, Kazakhstan
Corresponding author: aizat.dem@gmail.com

Abstract. *This study reports on high-angular-resolution observations of the massive star-forming region G328.2551−0.5321 obtained with the Atacama Large Millimeter/submillimeter Array at a wavelength of 0.89 mm. The innermost core structure is investigated by targeting high-excitation transitions of methanol, sulfur dioxide, and its sulfur-34 isotopologue. Analysis of the molecular emission reveals a compact and dense methanol component located at the continuum peak, which is surrounded by more extended emission from sulfur-bearing molecules. Kinematic analysis demonstrates a coherent velocity gradient along the major axis of the system. Position–velocity diagrams exhibit a characteristic butterfly morphology, which is consistent with the presence of a Keplerian rotation. Numerical model fitting provides dynamical mass estimates of approximately twenty solar masses for the central object, confirming the existence of a massive, rotating disk-like structure. Rotational diagram analysis of methanol transitions yields a rotational temperature of 187.9 ± 23.7 Kelvin and a total column density of 4.27 × 10¹⁶ cm⁻², indicating the presence of a hot molecular core. These findings suggest that a high-mass protostar is actively accreting within a compact disk-envelope system embedded in a hot core environment. The results contribute to the understanding of the physical conditions and gas dynamics in the early stages of massive star formation.*

Keywords: star formation, ALMA millimeter/submillimeter interferometry, hot molecular core, individual object G328.2551–0.5321.

1. Introduction

Understanding the earliest stages of massive star formation is essential for constraining how these objects shape the physical, chemical, and dynamical evolution of their natal environments. Massive stars profoundly influence their surroundings through radiative, mechanical, and chemical feedback, yet the physical conditions and internal kinematics of the dense gas from which they form remain incompletely understood [1].

Observational studies using a wide range of molecular tracers have significantly advanced our knowledge of massive star-forming regions. Species such as NH_3 [2-4] and H_2CO [5,6] are widely used to diagnose gas temperature and density. Other molecules, including HNCO, SiO, and HC_3N, trace shocks, outflows, and chemical enrichment associated with massive protostellar activity [7]. These studies highlight that molecular lines provide a powerful means of probing the physical conditions and energetics in dense molecular clouds.

Kinematic studies play a central role in revealing the dynamical processes governing massive star formation. Infall motions, rotation, and large-scale accretion flows are key indicators of early gravitational collapse [8]. Many massive star-forming regions exhibit complex hub–filament networks, where converging flows feed material into central dense cores [9-11]. Signatures of bipolar outflows, traced by molecules such as SiO or CO, further demonstrate the dynamic nature of these systems. Feedback from nearby massive stars, including expanding H II regions, may additionally trigger or regulate subsequent star formation. Cloud–cloud or core–core collisions have also been proposed as mechanisms for generating dense massive cores [12,13]. Additionally, the study of high-energy phenomena such as gamma-ray bursts, including early-time optical spectral measurements of events like GRB 200925B, provides further insights into the late-stage evolution and explosive feedback of the most massive stars [14].

Despite this progress, the initial conditions of massive protostellar evolution – particularly in *mid-infrared-quiescent,* deeply embedded clumps – remain poorly constrained. In such early phases, hot molecular cores may already be forming, but the heating, chemistry, and kinematics at <1000 AU scales are still largely unknown [15]. Probing these regions requires molecular lines that selectively trace warm, dense gas close to the protostar. High-excitation transitions of SO_2, CH_3OH, and ^{34}SO are particularly well suited for this purpose, as they originate in hot cores and are sensitive to rotational motions and disk-like structures.

The target of this study, G328.2551−0.5321, provides an excellent laboratory for examining these processes. It is the only massive object embedded within the infrared dark cloud MSXDC G328.25−00.51, located at a distance of 2.5 kpc. The source was initially identified at 870 μm in the ATLASGAL survey [16-18] and later followed up with ALMA as part of the SPARKS project (Search for High-mass Protostars with ALMA Revealed up to Kilo-parsec Scales. Its systemic velocity of −43.1 km s^{-1} [19-20] and its mid-infrared quiescent nature strongly suggest a very early evolutionary stage, possibly preceding the emergence of an ultracompact H II region. Evidence for complex internal motions further indicates active mass accretion within the core. Furthermore, ALMA observations of the environments of G301.1364-00.2249A and G333.0162+00.7615 have revealed compact molecular cores with clear velocity gradients, indicating that rotational motion is a common feature of hot cores in the earliest stages of high-mass star formation [21, 22].

In this work, we present high-angular-resolution ALMA Band 7 observations of G328.2551−0.5321 targeting highly excited transitions of SO_2, CH_3OH and ^{34}SO. These molecular tracers allow us to investigate the small-scale kinematics and physical conditions of the hot molecular gas surrounding the high-mass protostar. Our analysis aims to characterize rotational structure, identify signatures of infall or disk-like motions, and provide new constraints on the earliest phases of massive star formation within this quiescent infrared dark cloud.

2. Observations and data reduction

The data analyzed in this study were retrieved from the Atacama Large Millimeter/submillimeter Array (ALMA) archive. Observations toward the star-forming region G328.2551−0.5321 (phase center: R.A. (J2000) = $15^h57^m59.791^s$, Dec. (J2000) = −53°58′00.560″) were carried out under project code 2018.1.01679.S between 2019 April 16 and 21. The array configuration provided baselines ranging from 37.7 m (L5) to 281.4 m (L80), yielding a maximum recoverable scale of 5.16″ and a primary beam of 17.06″. The total on-source integration time was 1632.96 s (≈ 0.45 hr), resulting in a synthesized beam size of 0.487″.

The correlator was configured to cover the 333.468–349.091 GHz frequency range (ALMA Band 7) with a total bandwidth of 16 GHz and a spectral resolution of 0.977 MHz, corresponding to a velocity resolution of 0.487 km s^{-1}. The achieved continuum sensitivity was 0.074 mJy $beam^{-1}$.

The raw visibility data were processed using the standard ALMA calibration pipeline (Pipeline-CASA54-P1-B, CASA version 5.4.0-70 42254M), which applies standard bandpass, flux and phase calibrations. The resulting calibrated measurement set was subsequently imaged and self-calibrated in the Common Astronomy Software Applications package (CASA) [23] to improve the signal-to-noise ratio.

3. Results and discussion

The 0.89 mm continuum emission toward G328.2551–0.5321 is shown in Figure 1. Continuum contours are drawn at 0.00267, 0.00405, 0.00615, 0.00934, 0.01418, 0.02152, 0.03267, and 0.04960 Jy $beam^{-1}$. The beam, indicated by the black ellipse in the lower-left corner, represents the angular resolution, while the white plus marks the continuum peak. From a two-dimensional Gaussian fit to the continuum emission performed in

CARTA, we derive a peak position of R.A. (J2000) = $15^h57^m59.799^s$ and Dec. (J2000) = −53°58′00.528″ ± 0.0043″. The fitted peak flux density is 0.0496 ± 0.0055 Jy beam^{-1}, with a deconvolved source size of 0.099 ± 0.010″ × 0.134 ± 0.016″ (major × minor axis). The integrated flux density is 0.141 ± 0.020 Jy.

Several masers and young stellar object (YSO) candidates are overlaid on the continuum map: Class I and II methanol masers and an OH maser are shown as colored triangles [24,25] the IRAS 15541–5349 YSO candidate is indicated with an orange dot, the extended green object (EGO) G328.25–0.53 is shown as a green dot and the massive core G328.2551–00.5321–MM1 is marked with a brown dot [26]. These objects are associated with the 0.89 mm continuum emission, but none of them coincides exactly with the continuum peak.

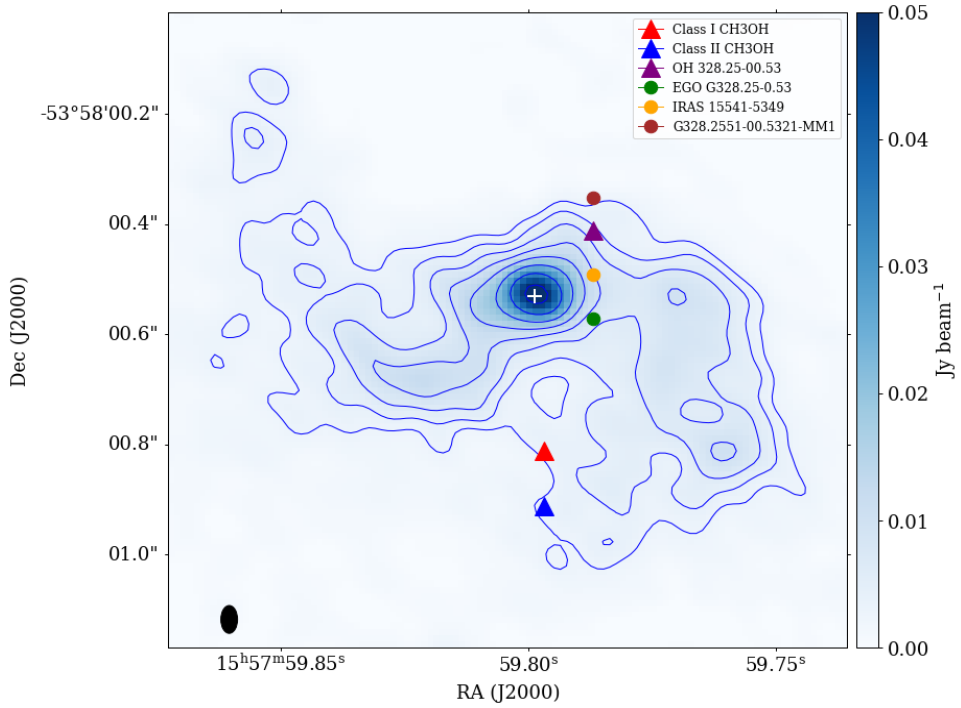

Fig.1. Continuum map toward G328.2551–0.5321 at 0.89 mm.

Figure 2 shows spectra of the SO_2 ($16_{4,12}$–$16_{3,13}$), CH_3OH ($12_{1,11}$–$12_{0,12}$ A) and ^{34}SO (7_8–6_7) molecular lines. Spectra taken directly at the continuum peak show noticeable asymmetry, likely caused by complex kinematic and structural effects near the emission maximum. To obtain representative line profiles, spectra were extracted from positions slightly offset from the continuum peak. These positions correspond to the intensity peaks of each molecular line in the integrated maps and cover regions about one synthesized beam in size. Gaussian profiles were fitted to all detected transitions. The spectral extraction and visualization were performed using CARTA [27]. The derived central upper-state energy (E_{up}/k), velocity (V_{LSR}), peak intensity (I_p) and full width at half maximum (FWHM; ΔV) are listed in Table 1.

Table 1. Observed line parameters toward G328.2551−0.5321

Molecule	Transition	Rest frequency (GHz)	E_u /k (K)	V_{LSR} (km/s)	I_p (Jy beam $^{-1}$)	ΔV (km s^{-1})
SO_2	16(4,12)–16(3,13)	346.523	166	−45.5 ± 0.12	0.7 ± 0.01	15 ± 0.3
CH_3OH	12(1,11)-12(0,12)A	336.864	197	−42.7 ± 0.06	0.8 ± 0.01	8.9 ± 0.14
^{34}SO	7(8) – 6(7)	333.902	81	−45.3 ± 0.07	0.29 ± 0.01	5.7 ± 0.17

Spectra extracted directly at the continuum peak exhibit noticeable asymmetry, likely due to complex kinematic and structural effects near the emission maximum. To obtain representative line profiles unaffected by these asymmetries, spectra were extracted from positions slightly offset from the continuum peak. These offsets correspond to the intensity maxima of each molecular line in the integrated maps and were taken from regions approximately one synthesized beam in size.

.

Figure 2 presents the averaged spectra of SO_2, CH_3OH, and ^{34}SO together with their Gaussian fits. The SO_2 line shows a slightly structured peak, with two closely spaced components, yet the profile remains broadly symmetric around the systemic velocity. The CH_3OH spectrum is well reproduced by a single Gaussian, exhibiting smooth and comparable blue and red wings. The optically thin ^{34}SO line displays a clean, symmetric Gaussian profile, indicating that it traces the intrinsic velocity field without significant radiative-transfer distortions. The generally symmetric shapes of all three lines suggest that the gas motions are dominated by ordered large-scale dynamics rather than irregular or multi-component structures.

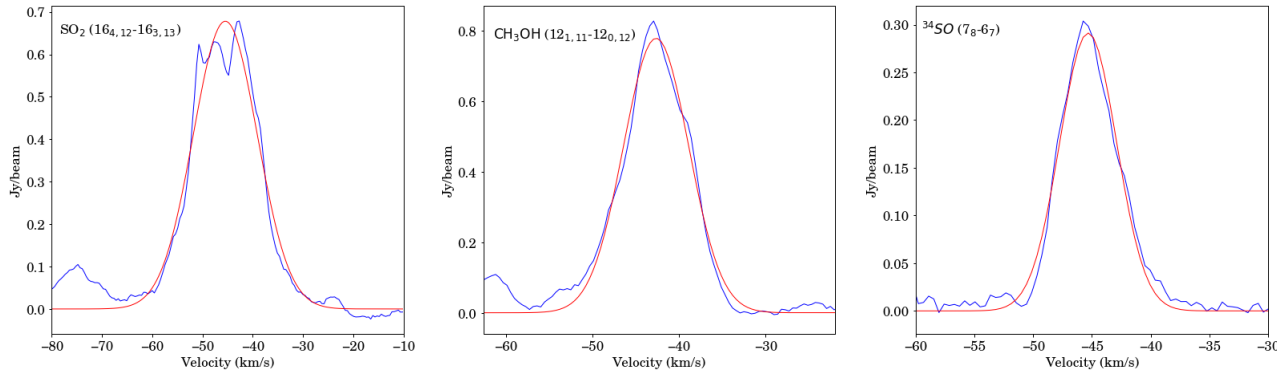

Fig.2. Molecular spectra with overlaid Gaussian fits. The blue curves represent the observed ALMA spectra, and the red curves show the multi-Gaussian fits.

Figure 3 shows the moment maps of integrated intensity, velocity and velocity dispersion, corresponding to moments 0, 1 and 2, of the $SO_2(16_{4,12}–16_{3,13})$, CH_3OH ($12_{1,11}–12_{0,12}$ A) and ^{34}SO ($7_8–6_7$) emissions toward the G328.2551-0.5321 core. In the moment 0 map, the CH_3OH emission peak is shifted 0.089″ northeast of the continuum peak, with an integrated intensity of 12 Jy beam^{-1} km s^{-1}, whereas the ^{34}SO peak is offset 0.082″ to the northwest, reaching 4 Jy beam^{-1} km s^{-1}. The SO_2 emission peak coincides with the continuum peak and extends northward, attaining an integrated intensity of 15 Jy beam^{-1} km s^{-1}. The moment-1 maps of SO_2 ($16_{4,12}–16_{3,13}$; velocity range −51 km s^{-1} to −44 km s^{-1}) and ^{34}SO ($7_8–6_7$; velocity range −48 km s^{-1} to −39 km s^{-1}) display smooth west (blue-shifted) to east 4 (red-shifted) velocity gradients along PA = 98°, consistent with organized rotation. The corresponding moment-2 maps show enhanced turbulence near the core centers, with values of ~ 4–5 km^2 s^{-2} for SO_2 and ~ 10–15 km^2 s^{-2} for ^{34}SO. Both SO_2 and ^{34}SO show extended molecular line emission, indicating that these molecules are distributed over a relatively large region. In contrast, CH_3OH ($12_{1,11}–12_{0,12}$ A) exhibits compact emission coincident with the continuum peak, with a central velocity dispersion of ~7–7.5 km^2 s^{-2} that decreases outward, consistent with the findings of [25].

This compact morphology, spectral lines**,** combined with the observed velocity gradient, strongly supports the presence of a rotating structure, such as a circumstellar disk. To verify the velocity gradient seen in the moment-1 maps, a position–velocity (PV) diagram was extracted along PA = 98°, confirming that the emission follows the NE–SW direction.

Figure 4 presents the PV diagrams of the massive star-forming region G328.2551–0.5321 for the CH_3OH ($12_{1,11}–12_{0,12}$ A) and SO_2 ($16_{4,12}–16_{3,13}$) transitions. The velocity axes span roughly −55 km s^{-1} to −35 km s^{-1} for CH_3OH and −60 km s^{-1} to −35 km s^{-1} for SO_2. The systemic velocities, indicated by the dashed horizontal lines, are $V_0 \approx -45.135$ km s^{-1} for CH_3OH and $V_0 \approx -49.119$ km s^{-1} for SO_2. Similar PV structures observed in other massive cores, such as G333.6–0.2, exhibit clear velocity gradients along the major axis, providing strong evidence for the presence of rotating molecular envelopes or disk-like structures [28].

The dynamical mass (M_{dyn}) was estimated from the PV diagrams by applying the Keplerian rotation model, according to the following equation:

$$M_{dyn} = \frac{v^2 R}{G \sin^2 i} \quad (1)$$

where v is the observed rotation velocity at an offset R, G is the gravitational constant, and i is the inclination angle of the disk (taken as 53.7° in this work).

The uncertainty in the dynamical mass was estimated by considering the propagation of errors in the main parameters of the Keplerian model, including the rotational velocity, radial distance, and disk inclination angle. Based on typical uncertainties in these quantities, the resulting uncertainty in the dynamical mass is on the order of 10–15%.

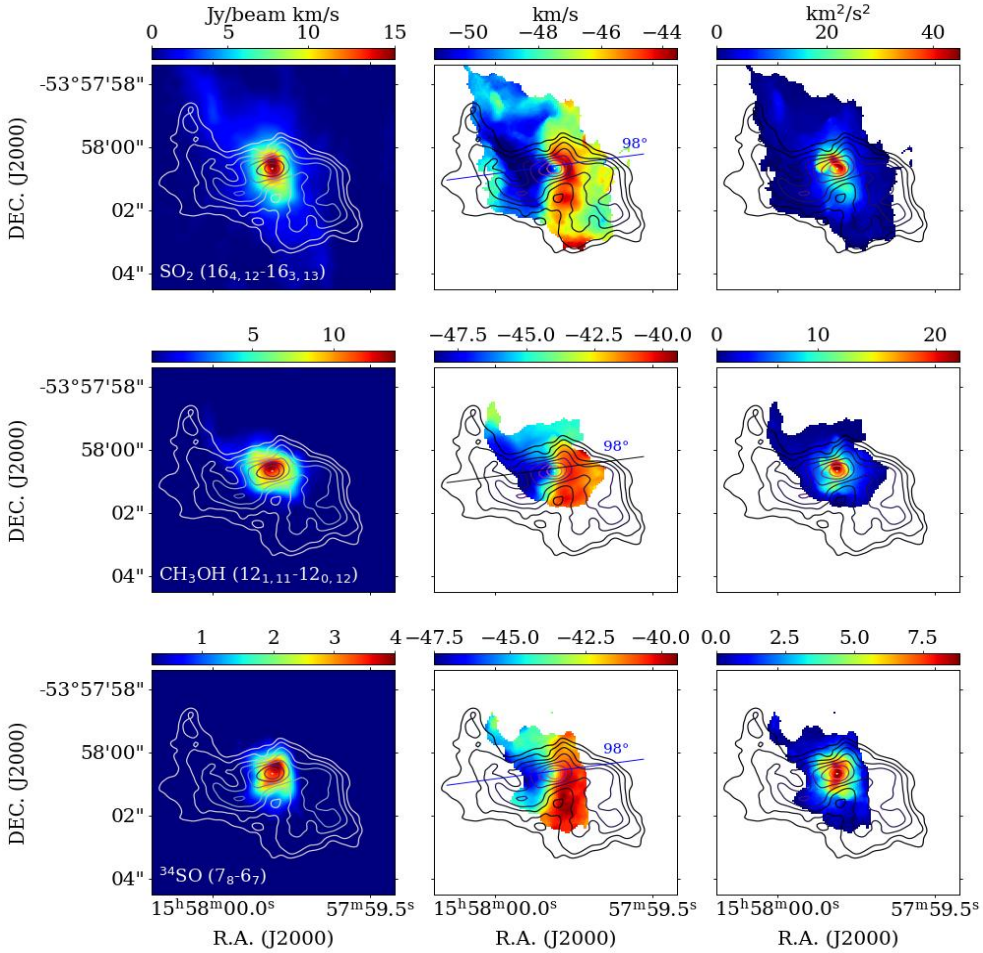

Fig.3. Moment 0, 1 and 2 maps of $SO_2(16_{4,12}–16_{3,13})$, CH_3OH ($12_{1,11}–12_{0,12}$ A) and ^{34}SO ($7_8–6_7$) emission toward G328.2551–0.5321 A. Contour levels are 0.00267, 0.00405, 0.00615, 0.00934, 0.01418, 0.02152, 0.03267 and 0.04960 Jy beam^{-1} km s^{-1}. The black ellipse in the lower-right panel denotes the synthesized beam.

The diagrams exhibit a pronounced, symmetric velocity gradient across the continuum major axis, with redshifted emission on one side and blue shifted emission on the other, producing the characteristic “butterfly” morphology expected for rotation. White curves on each panel represent a Keplerian disk model [29] with an inclination of $i \approx 53.7°$, which traces the bright emission ridge well. The inclination angle was derived from the deconvolved continuum ellipse. The fitted dynamical masses are $M \approx 20.5$ $M_\odot$ for CH_3OH and $M \approx 23.2$ $M_\odot$ for SO_2, indicating that the two tracers yield slightly different values. Small asymmetries in intensity and the presence of separate bright knots in SO_2 suggest that the two molecules likely trace somewhat different gas conditions or spatial regions within the rotating structure. These results are slightly higher but broadly consistent with the 10–20 $M_\odot$ range reported by [30], likely reflecting differences in tracer excitation and the adopted inclination.

Four transitions of CH_3OH have been detected toward G328.2551–0.5321. A rotation temperature diagram can therefore be used to estimate the rotational temperature and column density with Madrid Data CUBe Analysis.

The spectroscopic parameters of the detected CH_3OH transitions are listed in Table 2, including the transition designation, rest frequency, upper-state energy (E_{up}/k) and intensity. Figure 5 presents the rotational diagram for the methanol transitions observed toward the core.

.

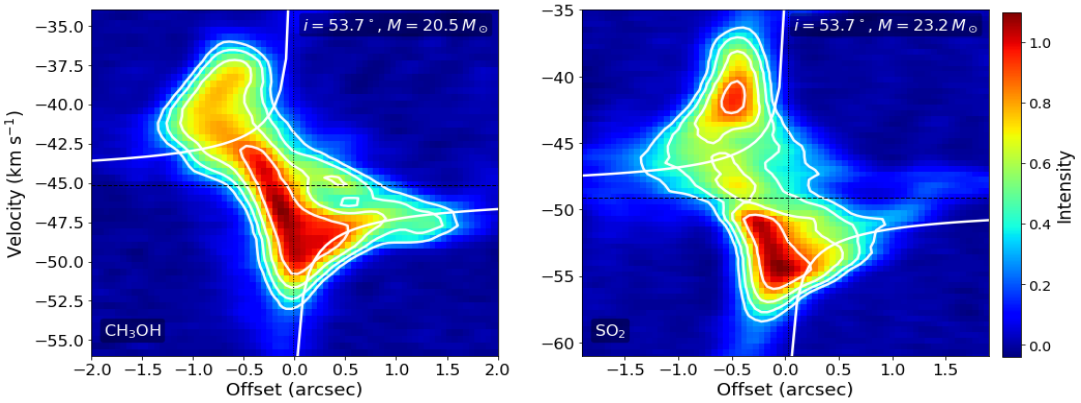

Fig.4. Position–velocity (PV) diagrams of the CH_3OH ($12_{2,11}$–$12_{0,12}$ A) and SO_2 ($16_{4,12}$–$16_{3,12}$) transitions toward G328.2551−0.5321, extracted along the major kinematic axis (i ≈ 53.7°). The white curves correspond to the Keplerian disk model.

Table 2. Parameters of CH_3OH (vt=0–2) molecular lines used for the rotational diagram analysis.

Molecule	Transitions	Rest Frequency (GHz)	E_{up}/k (K)	Peak intensity (K)	$\log_{10}(N_u/g_u)$
CH_3OH, vt=0–2	$3_{0,1}$–$2_{1,1}$	334.426571	125.51	0.53	5.7106
	$25_{3,1}$–$24_{2,1}$	334.679524	314.46	0.29	5.3496
	$2_{2,1}$–$3_{1,1}$	335.133570	1073.82	0.63	4.6465
	$9_{1,0}$–$8_{2,0}$	333.864722	44.67	0.05	5.6072

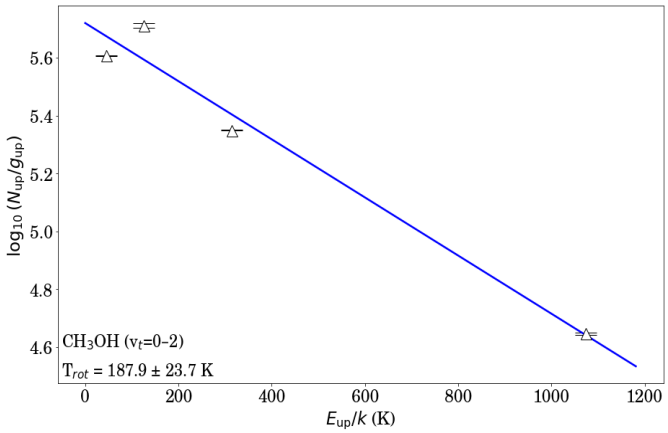

Fig.5. Rotational diagram of the observed CH_3OH transitions.

The uncertainties in the peak intensities, expressed as $\log_{10}(N_u/g_u)$ are indicated by triangles in the horizontal stripes of the data. The x-axis represents the upper-state energy E_{up}/k, expressed in Kelvin. A linear least-squares fit was applied to the data, yielding a rotational temperature of T_{rot} = 187.9 ± 23.7 K and a total column density of N = 4.27 × 10^{16} cm^{-2}. The uncertainty in the rotational temperature was derived directly from the standard error of the slope in the linear least-squares fit. Equation (2) demonstrates that the logarithm of the upper-level population normalized by its degeneracy, log (N_u/g_u), varies linearly with the upper-level energy E_u.

By plotting log (N_u/g_u) as a function of E_u/k_B, a linear fit can be applied to derive two key physical parameters: the rotational temperature from the slope and the total column density from the intercept.

$$log\left(\frac{N_u^{thin}}{g_u}\right) = -\left(\frac{log e}{T_{rot}}\right)\left(\frac{E_u}{k_B}\right) + log\left(\frac{N_{total}}{Q(T_{rot})}\right) \quad (2)$$

In this approach, N_u/g_u is calculated from the observed line intensities using the rotational diagram method under the assumptions of local thermodynamic equilibrium (LTE) and optically thin emission. Accordingly,

in the rotational diagram, the X-axis represents the upper-level energy E_u/k_B (in K), while the Y-axis corresponds to $\log(N_u/g_u)$, the logarithm of the column density per statistical weight [31].

4. Conclusion

High-angular-resolution ALMA observations of emission from highly excited molecular lines of CH_3OH, ^{34}SO and SO_2 toward the massive star-forming region G328.2551−0.5321 were carried out. The main results and conclusions are summarized below.

The 0.89 mm continuum peak of G328.2551−0.5321, together with surrounding Class I and II CH_3OH and OH masers, IRAS 15541–5349, EGO G328.25–0.53 and the massive core G328.2551−00.5321−MM1, reveals a complex, heterogeneous star-forming environment in which different tracers map distinct physical conditions and evolutionary stages around a central hub.

The moment-0 maps of molecular gas show that the molecular emission peaks are offset from the continuum peak. SO_2 and ^{34}SO are spatially extended across the envelope, whereas the CH_3OH emission is compact and centered on the continuum peak, indicating that methanol traces the densest and most compact region of the core.

The moment-1 maps of SO_2, CH_3OH and ^{34}SO reveal smooth and well-defined velocity gradients oriented from west (blue-shifted) to east (red-shifted) along PA = 98°, confirming the presence of an organized rotational motion within the core.

The position–velocity (PV) diagrams reveal a characteristic “butterfly”-shaped morphology, indicative of Keplerian rotation around a central massive source. Keplerian model fits yield dynamical masses of $M \approx 20.5$ $M_\odot$ for CH_3OH and $M \approx 23.2$ $M_\odot$ for SO_2, confirming the presence of a massive, rotating disk-like structure.

Rotational transitions of CH_3OH (v_t = 0–2) were detected toward G328.2551–0.5321. The rotational temperature is $T_{rot} = 187.9 \pm 23.7$ K and the total column density is $N = 4.27 \times 10^{16}$ cm^{-2}, indicating the presence of warm and dense gas characteristic of a hot molecular core.

These results demonstrate that G328.2551−0.5321 hosts a hot molecular core with a rotating disk, representing an active site of massive star formation.

Conflict of interest statement

The authors declare that they have no conflict of interest in relation to this research, whether financial, personal, authorship or otherwise, that could affect the research and its results presented in this paper.

CRediT author statement

Islyam Zh.B.: Conceptualization, Software, Writing - Original Draft; **Nodyarov A.S.:** Investigation, Formal analysis; **Demessinova A.M.:** Methodology, Validation; **Manapbayeva A.B.:** Visualization, Resources; **Kyzgarina M.T.:** Supervision, Writing - Review & Editing; **Zhumabay N.:** Data Curation, Software. The final manuscript was read and approved by all authors.

Funding

This research has been funded by the Science Committee of the Ministry of Science and Higher Education of the Republic of Kazakhstan (grant no. AP26102915)

Acknowledgements

This paper makes use of the following ALMA archival data: ADS/JAO.ALMA#2018.1.01679. S. ALMA is a partnership of ESO (representing its member states), NSF (USA), and NINS (Japan), together with NRC (Canada), MOST and ASIAA (Taiwan), and KASI (Republic of Korea), in cooperation with the Republic of Chile. The Joint ALMA Observatory is operated by ESO, AUI/NRAO, and NAOJ.

References

1 Nummelin A., Bergman P., Hjalmarson Å., Friberg P., Irvine,W. M., Millar T. J., Ohishi M., & Saito S. (2000) A three-position spectral line survey of Sagittarius B2 between 218 and 263 GHz. II. Data analysis. *The Astrophysical Journal Supplement Series*, *128*(1), 213–243. https://doi.org/10.1086/313376

2 Dunham M. K., Rosolowsky E., Evans N.J., II, Cyganowski C., & Urquhart J. S. (2011) The Red MSX Source survey: Ammonia and water maser analysis of massive star-forming regions. *The Astrophysical Journal*, *741*(2), 110–136. https://doi.org/*doi:10.1088/0004-637X/741/2/110*

.

3 Berdikhan D., Esimbek J., Henkel C., Zhou J., Tang X., Liu T., Wu G., Li D., He Y., Komesh T., Tursun K., Zhou D., Imanaly E., & Jandaolet Q. (2024) Ammonia observations of Planck cold cores. *Astronomy & Astrophysics*, *684*, A144. https://doi.org/10.1051/0004-6361/202348381

4 Sailanbek S., Esimbek J., Henkel C., Sobolev A. M., Ladeyschikov D. A., Berdikhan D., Wu G., Zhou J., Tang X., He Y., Li D., Tursun K., Zhou D., Ma Y., Komesh T., Ibraimov M., & Adilzhan K. (2025) Ammonia survey of the BGPS sources with the Nanshan 26-m telescope. *Monthly Notices of the Royal Astronomical Society*, *539*(4), 2987–3012. https://doi.org/10.1093/mnras/staf564

5 Imanaly E., Esimbek J., Baan W., Wu G., Zhou J., Li D., Tang X., He Y., Komesh T., Zhou D., Tursun K., Ma Y., Berdikhan D., Sobolev A. M., & Jandaolet Q. (2025) Formaldehyde in the Cygnus-X region. *Monthly Notices of the Royal Astronomical Society*, *542*(3), 2074–2086. https://doi.org/10.1093/mnras/staf1346

6 Komesh T., Esimbek J., Baan W., Zhou J., Li D., Wu G., He Y., Sailanbek S., Tang X., & Manapbayeva A. (2019) H_2CO and H110α observations toward the Aquila molecular cloud. *The Astrophysical Journal*, *874*(2), 172. https://doi.org/10.3847/1538-4357/ab0ae3

7 He Y.X., Henkel C., Zhou J. J., Esimbek J., Stutz A. M., Liu H. L., Ji W. G., Li D. L, Wu G., Tang X. D., Komesh T., & SailanbekS (2021) Extended HNCO, SiO, and HC_3N emission in 43 southern star-forming regions. *The Astrophysical Journal Supplement Series*, *253*(2), 44. https://doi.org/10.3847/1538-4365/abd0fb

8 Komesh T., Garay G., Henkel C., Omar A., Estalella R., Assembay Z., Li D., Guzmán A., Esimbek J., Huang J., He Y., Alimgazinova N., Kyzgarina M., Bekdaulet S., Zhumabay N., & Manapbayeva A. (2024) Infall motions in the hot core associated with the hypercompact H II region G345.0061+01.794 B. *The Astrophysical Journal*, *967*(1), 15. https://doi.org/10.48550/arXiv.2307.07459

9 Treviño-Morales S. P., Fuente A., Sánchez-Monge Á., Kainulainen J., Didelon P., Suri S., Schneider N., Ballesteros-Paredes J., Lee Y., Hennebelle P., Pilleri P., González-García M., Kramer C., García-Burillo S., Luna A., Goicoechea J., Tremblin P., Geen S. (2019) Dynamics of cluster-forming hub-filament systems: The case of the high-mass star-forming complex Monoceros R2. *Astronomy & Astrophysics*, *629*, A81. https://doi.org/10.1051/0004-6361/201935260

10 Zhang W., Zhou J., Esimbek J., Baan W., He Y., Tang X., Li D., Ji W., Wu G., Ma Y., Li J., Zhou D., Tursun K., & Komesh T. (2024) Kinematics and star formation of hub-filament systems in W49A. *Astronomy & Astrophysics*, *688*, A99. https://doi.org/10.1051/0004-6361/202348580

11 Ma Y., Zhou J., Esimbek J., Baan W., Li D., Tang X., He Y., Ji W., Zhou D., Wu G., Tursun K., & Komesh T. (2023). Gravitational collapse and accretion flows in the hub filament system G323.46-0.08. *Astronomy & Astrophysics*, *676*, A15. https://doi.org/10.1051/0004-6361/202346248

12 Li D., Henkel C., Kraus A., Tang X., Baan W., Esimbek J., Wang K., Wu G., Liu T., Sobolev A. M., Zhou J., He Y., & Komesh T. (2025) Evidence for core–core collision in Barnard 68. *The Astrophysical Journal*, *985*(2), 230. https://doi.org/10.3847/1538-4357/add326

13 Berdikhan D., Esimbek J., Henkel C., Zhou J., Tang X., Liu T., Wu G., Li D., He Y., Komesh T., Tursun K., Zhou D., Imanaly E., & Jandaolet Q. (2024) Ammonia observations of Planck cold cores. *Astronomy & Astrophysics*, *684*, A144. https://doi.org/10.1051/0004-6361/202348381

14 Abdullayev Z., Komesh T., Grossan B., Abdikamalov E., Maksut Z., Krugov M., Myrzakul S., & Tuiakbayeva D. (2025) Early-time optical spectral shape measurements of GRB 200925B. *Revista Mexicana de Astronomía y Astrofísica (Serie de Conferencias)*, *59*, 109–113. https://doi.org/10.22201/ia.14052059p.2025.59.20

15 Shimonishi T., Das A., Sakai N., Tanaka K. E. I., Aikawa Y., Onaka T., Watanabe Y., & Nishimura Y. (2020) Chemistry and physics of a low-metallicity hot core in the Large Magellanic Cloud. *The Astrophysical Journal*, *891*(2), 164. https://doi.org/10.3847/1538-4357/ab6e6b

16 Schuller F., Menten K. M., Contreras Y., Wyrowski F., Schilke P., Bronfman L., Henning T., Walmsley C. M., Beuther H., Bontemps S., Cesaroni R., Deharveng L., Garay G., Herpin F., Lefloch B., Linz H., Mardones D., Minier V., Molinari S., Motte F., Nyman L. Å., Reveret V., Risacher C., Russeil D., Schneider N., Testi L., Troost T., Vasyunina T., Wienen M., Zavagno A., KovacsA., Kreysa E., Siringo G., & Weiß A. (2009) ATLASGAL – The APEX Telescope Large Area Survey of the Galaxy at 870 μm. *Astronomy & Astrophysics*, *504*(2), 415–427. https://doi.org/10.1051/0004-6361/200811568

17 Csengeri T., Urquhart J. S., Schuller F., Motte F., Bontemps S., Wyrowski F., Menten K., Bronfman L., Beuther H., Henning T., Testi L., Zavagno A., & Walmsley M. (2014). The ATLASGAL survey: A complete sample of luminous clumps in the inner Galaxy. *Astronomy & Astrophysics*, *565*, A75. DOI:10.1051/0004-6361/201322434

18 Csengeri T., Bontemps S., Wyrowski F., Belloche A., Menten K. M., Leurini S., Beuther H., Bronfman L., Commerçon B., Chapillon E., Longmore S., Palau A., Tan J. C., & Urquhart J. S. (2018) ALMA survey of high-mass protostars revealed up to kilo-parsec scales (SPARKS). I. Indication for a centrifugal barrier in the environment of a single high-mass envelope. *Astronomy & Astrophysics*, *617*, A89. https://doi.org/10.1051/0004-6361/201832753

19 Csengeri T., Bontemps S., Wyrowski F., Megeath S. T., Motte F., Sanna A., Wienen M., & Menten K. M. (2017) The ATLASGAL survey: The sample of young massive cluster progenitors? *Astronomy & Astrophysics*, *601*, A60. https://doi.org/10.1051/0004-6361/201628254

20 Csengeri T., Belloche A., Bontemps S., Wyrowski F., Menten K. M., Bouscasse L. (2019) Search for high-mass protostars with ALMA revealed up to kilo-parsec scales. II. Complex organic molecules and heavy water in shocks around a young high-mass protostar. *Astronomy & Astrophysics*, *632*, A57. https://doi.org/10.1051/0004-6361/201935226

21 Assembay Zh., Komesh T., Garay G., Omar A., Esimbek J., Alimgazinova N., Kyzgarina M., & Murat Sh. (2022) ALMA observations of the environments of G301.1364-00.2249 A. *Proceedings of the Intern. Astronomical Union*, *18*(S380), 204–206. https://doi.org/10.1017/S1743921323002624

22 Komesh T., Omar A., Garay G., Assembay Z., Alimgazinova N., Zhumabay N., & Kyzgarina M. (2021) ALMA observations of the environments of G333.0162+00.7615. In T. Wong & W.-T. Kim, *Proceedings of the Intern.Astronomical Union*, 17, S362, 35–38. Cambridge University Press. https://doi.org/10.1017/S1743921323000121

23 McMullin J. P., Waters B., Schiebel D., Young W., & Golap K. (2007) *CASA architecture and applications. Astronomical Data Analysis Software and Systems XVI*, 376, 127. https://www.aspbooks.org/custom/publications/paper/

24 Caswell J. L., Fuller G. A., Green J. A., Avison A., Breen S. L., Brooks K. J., Burton M. G., Chrysostomou A., Cox J., Diamond P. J., Ellingsen S. P., Gray M. D., Hoare M. G., Masheder M. R. W., McClure-Griffiths N. M., Pestalozzi M. R., Phillips C. J., Quinn L., Thompson M. A., Voronkov M. A., Walsh A. J., Ward-Thompson D., Wong-McSweeney D., Yates J. A., & Cohen R. J. (2010) The 6-GHz methanol multibeam maser catalogue – I. Galactic Centre region, longitudes 345° to 6°. *Monthly Notices of the Royal Astronomical Society*, *404*(2), 1029–1060. https://doi.org/10.1111/j.1365-2966.2010.16339.x

25 McCarthy T., Ellingsen S., Breen S. L., Voronko M. A., Chen X. (2018). Detection of 84 GHz Class I methanol maser emission toward NGC 253. *The Astrophysical Journal Letters*, *867*(1), L4. https://doi.org/10.3847/2041-8213/aae82c

26 Csengeri T., Bontemps S., Wyrowski F., Megeath S. T., Motte F., Sanna A., Wienen M., & Menten K. M. (2017) The ATLASGAL survey: The sample of young massive cluster progenitors? *Astronomy & Astrophysics*, *601*, A60. https://doi.org/10.1051/0004-6361/201628254

27 Cartavis. https://cartavis.org/ (accessed November 5, 2025).

28 Omar A., Abdirakhman A., Alimgazinova N., Kyzgarina M., Naurzbayeva A., Islyam Z., Turekhanova K., Demessinova A., & Manapbayeva A. (2025) ALMA observations of G333.6-0.2: Molecular and ionized gas environment. *Galaxies*, *13*(4), 73. https://doi.org/10.3390/galaxies13040073

29 Bosco F., Beuther H., Ahmadi A., Mottram J. C., Kuiper R., Linz H., Maud L., Winters J. M., Henning T., Feng S., Peters T., Semenov D., Klaassen P. D., Schilke P., Urquhart J. S., Beltrán M. T., Lumsden S. L., Leurini S., Moscadelli L., Cesaroni R., Sánchez-Monge Á., Palau A., Pudritz R., Wyrowski F., & Longmore S. (2019) Fragmentation, rotation, and outflows in the high-mass star-forming region IRAS 23033+5951: A case study of the IRAM NOEMA large program CORE. *Astronomy & Astrophysics*, *629*, A10. https://doi.org/10.1051/0004-6361/201935318

30 Csengeri T., Bontemps S., Wyrowski F., Belloche A., Menten K. M., Leurini S., Beuther H., Bronfman L., Commerçon B., Chapillon E., Longmore S., Palau A., Tan J. C., & Urquhart J. S. (2018) Search for high-mass protostars with ALMA revealed up to kilo-parsec scales I. Indication for a centrifugal barrier in the environment of a single high-mass envelope. *Astronomy & Astrophysics*, *617*, A89. https://doi.org/10.1051/0004-6361/201832753

31 Martín S., Martín-Pintado J., Blanco-Sánchez C., Rivilla V. M., Rodríguez-Franco A., & Rico-Villas F. (2019) Spectral line identification and modelling (SLIM) in the Madrid Data CUBe analysis package: Interactive software for data cube analysis. *Astronomy & Astrophysics*, *631*, A159. https://doi.org/10.1051/0004-6361/201936144

AUTHORS' INFORMATION

Islyam, Zh.B. — Master's student, Faculty of Physics and Technology, Al-Farabi Kazakh National University, Almaty, Kazakhstan; Scopus Author ID: 60077235000; https://orcid.org/0009-0006-5496-4501; islyamovzhomart@gmail.com

Nodyarov, A.S. – PhD, Senior Lecturer, Al-Farabi Kazakh National University, Almaty, 050040, Kazakhstan, Scopus Author ID: 57893764100; https://orcid.org/0000-0002-0045-5457; nodyarov.atilkhan@gmail.com.

Demessinova, A.M. — PhD, Senior lecturer, Faculty of Physics and Technology, Al Farabi Kazakh National University, Almaty, Kazakhstan; Scopus Author ID: 57211859262; https://orcid.org/0000-0001-5049-9338; aizat.dem@gmail.com

Manapbayeva, A.B. — Senior Researcher, Institute of Experimental and Theoretical Physics; Senior lecturer, Kazakh National Women's Teacher Training University, Almaty, Kazakhstan; Scopus Author ID: 57205165517; https://orcid.org/0000-0002-0322-1509; manapbayeva.arailym@gmail.com

Kyzgarina, M.T. — PhD, Senior lecturer, Faculty of Physics and Technology, Al Farabi Kazakh National University, Almaty, Kazakhstan; Scopus Author ID: 35146124400; https://orcid.org/0000-0002-4103-7657; meir83physics@gmail.com

Zhumabay, N — PhD student, Abai Kazakh National Pedagogical University, Almaty, Kazakhstan; Scopus Author ID: 58420497400; https://orcid.org/0009-0008-7100-008X; nurman-0906@mail.ru

.